RSC Advances

ROYAL SOCIETY OF CHEMISTRY

www.rsc.org/advances

RSC Advances

Dynamic Article Links ►

Cite this: DOI: 10.1039/c0xx00000x

www.rsc.org/xxxxxx

Communication

Reasons Behind the Improved Thermoelectric Properties of Poly(3-hexylthiophene) Nanofiber Networks

B. Endrődi,[a, b] J. Mellár,[c] Z. Gingl,[c] C. Visy,[a] and C. Janáky*[,a, b]

Received (in XXX, XXX) Xth XXXXXXXXX 20XX, Accepted Xth XXXXXXXXX 20XX
DOI: 10.1039/b000000x

Enhanced thermoelectric properties of poly(3-hexylthiophene) nanofiber networks, doped in their reaction with silver cations are presented. The role of charge carrier concentration and mobility (influenced by the supramolecular structure and nanoscale morphology) is discussed. The nanonet structure leads to a six fold increase in the ZT value compared to the bulk polymer counterpart.

Thermoelectric power generation is an attractive and environmentally friendly way to recover energy from industrial or communal waste heat.[1] Most frequently, inorganic semiconductors – mostly alloys or intermetallics, composed of elements like Pb, Bi, Te, Sn, Si – are employed in this vein.[2] High cost and moderate room temperature efficiencies of these materials necessitates the better understanding of the basic principles (related to both chemical composition and morphological parameters) as well as the search for new materials.

Because of their low thermal conductivity (κ) and remarkably high Seebeck coefficient (S) (in their neutral form), intrinsically conducting organic polymers (CPs) are possible cheap alternatives for thermoelectric applications. Thermoelectric characterization and optimization of different CPs have been performed,[3] but none of them could reach the thermoelectric figure of merit (ZT) of their best inorganic counterparts yet. Best ZT values, approaching 0.5 in the case of PEDOT-Tosylate and PEDOT-PSS systems however, hold great promise for organic thermoelectrics.[4,5] Outstanding performance of these two PEDOT systems is mostly facilitated by their metallic (or semi-metallic) electrical conductivity (σ).[6] On the other hand, the highest Seebeck-coefficients – besides the unstable polyacetylene – have been reported for poly(3-alkylthiophene)s, but their practical utilization is hampered by their low electrical conductivity.[7,8]

Several strategies can be envisioned to increase the low conductivity of the CPs. Probably the most obvious approach is the oxidation of the polymer (doping): increment of the charge carrier concentration results in higher electrical conductivity. Note however, that charge carrier density affects electrical- and thermal conductivity, and the Seebeck coefficient oppositely: parallel to the increase in conductivity, Seebeck coefficient drops rapidly, while thermal conductivity slightly increases.[3] Consequently, for most CPs, there is an optimal doping level, where ZT reaches its maximum value.[3,4]

Different tactics have been developed to circumvent the strict co-dependency of the above parameters. First, incorporation of highly conductive nano-objects into the CP matrix may have significant contribution to the electrical conductivity, but just a slight undesirable influence on the Seebeck coefficient.[7,9,10] In a sophisticated variant of the previous approach, the conductive nanomaterial originates from the doping process (e.g., when noble metal ions are used as dopants).[11-13] In such methods, conductive metal nanoparticles, grown in situ on the CP surface, are „by-products" of the doping reaction.

Finally, another viable strategy is to increase charge carrier mobility. On one hand, this can be achieved by the rational design of the molecular structure of the polymers (inspired by the organic electronics community), resulting in high hole-, or electron mobility.[14-16] Alternatively, carefully engineered supramolecular structure and morphology may also contribute to improved electrical properties. For example, nanofiber formation resulted in enhanced electrical conductivities for certain CPs.[17-19] Formation of such highly-ordered structures facilitates electron hopping between polymer chains leading to free electron pathways along the longitudinal dimension of the nanofibers.

In this study, we demonstrate an efficient way to exploit the synergistic combination of the above mentioned strategies to maximize ZT, using poly(3-hexylthiophene) (P3HT) as a model system. Self-assembled networks of P3HT nanofibers (nanonets) were formed and subsequently doped by silver perchlorate, to tune their oxidation level. Careful control over both the doping process and the morphology (compact film vs. nanonet) allowed the evaluation of the individual contribution of the above strategies.

[a] Department of Physical Chemistry and Materials Science, University of Szeged, Rerrich Square 1., Szeged, H-6720, Hungary

[b] MTA-SZTE „Lendület" Photoelectrochemistry Research Group, Rerrich Square 1,Szeged, H-6720, Hungary

[c] Department of Technical Informatics, University of Szeged, Árpád Square 2., Szeged, H-6720, Hungary

*E-mail: janaky@chem.u-szeged.hu; Fax: +36 62 546-482 Tel: +36 62 544-111

† Electronic Supplementary Information (ESI) available: [Detailed experimental procedures, XRD, UV-Vis, SEM, Raman, FT-IR and thermoelectric characterization]. See DOI: 10.1039/c000000x/

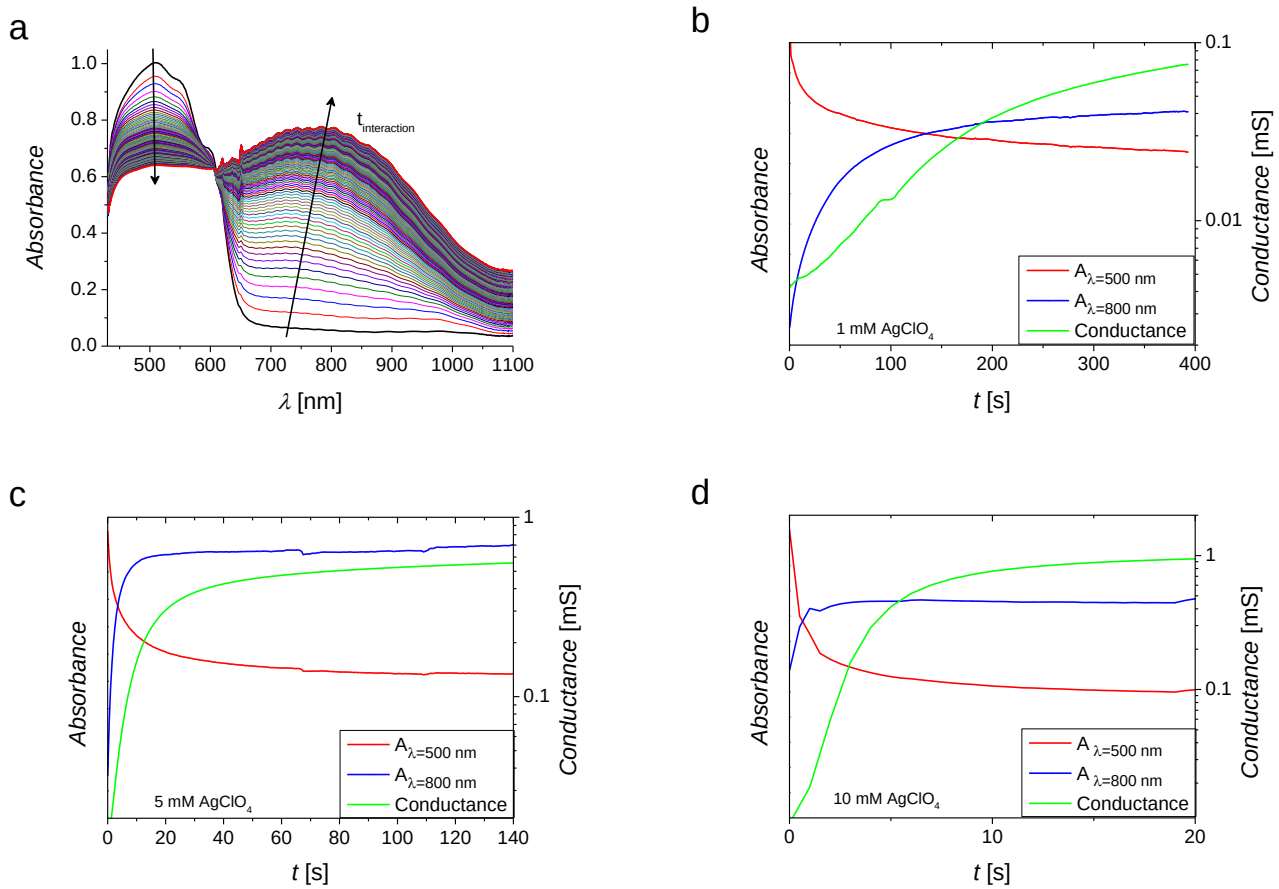

Figure 1. (a) Changes on the UV-Vis spectrum of P3HT during doping process (1 mM $AgClO_4$, Δt = 2 s); (b-d) Simultaneous *in situ* spectroelectrochemical and conductance changes during the doping process at 1 mM, 5mM and 10 mM $AgClO_4$ concentrations, respectively.

To optimize the thermoelectric performance of P3HT, fine tuning of its doping level is of prime importance. The key parameters of the doping reaction are the following: (i) the oxidant (both its chemical nature and concentration); (ii) the solvent; (iii) the reaction time. Using a silver salt as the oxidant, metallic Ag nanoparticles are formed on the polymer,[12,13] possibly contributing to the conductivity enhancement.

To gain mechanistic insights on the doping procedure, kinetics of the redox reaction was monitored by simultaneous *in situ* UV-Vis spectroscopy and conductance measurements.[20] As seen in Figure 1a, spectral changes indicate a redox reaction between P3HT and the silver cations. Very similarly to a spectro*electro*chemical experiment, gradual decrease of the absorption peak related to the neutral form (λ_{max}=510 nm) is accompanied by the increase in absorbance characteristic for the oxidized form (λ_{max}=780 nm).[21,22] Kinetics of the reaction was studied by transforming these spectra to time based plots, depicting the absorbance change registered at the above two characteristic wavelengths.

As seen in Figure 1b-d, increasing oxidant concentration leads to a rise in the reaction rate. In the case of the most concentrated solution (c_{Ag+}=10 mM), spectral changes reach saturation within a few seconds. For the other two concentrations, however, a much longer timescale can be witnessed, allowing more precise control over the doping process.

The most important conclusions derived from these experiments are the following: (i) the increase in conductance is always in delay to spectral changes; (ii) the time scale of the conductance change (speed of the doping process) is inversely proportional to the oxidant concentration; (iii) maximum value of conductivity is proportional to the oxidant concentration.

The redox reaction between P3HT and Ag^+ ions was further monitored by *ex situ* FT-IR- (Figure 2a) and Raman-spectroscopy (Figure S7). Before the doping reaction, characteristic vibrations of C-H groups can be observed between 2800-3000 cm^{-1}, while vibrations related to the thiophene rings appear below 1500 cm^{-1} in the infrared spectrum (Figure S5 and Table S1). As the doping reaction proceeds, characteristic tenor of the spectrum ceases gradually, indicating the formation of the oxidized, conducting form of P3HT.[12] Similarly, changes on the Raman spectrum of the P3HT due to the doping also indicates the oxidation of the polymer backbone. The shift in the peak, related to the C_α=C_β stretching, and the changes in the relative intensities all confirm the presence of heavily doped form of the P3HT (See S6 for further information). [23]

Supramolecular structure of P3HT nanofibers was investigated by XRD (Figure 2b and Figure S7). The nanofibrillar P3HT shows sharp reflections *only*, instead of a broad, hill-type reflection typically observed for regiorandom P3HT obtained by chemical polymerization. This can be attributed to a highly-ordered structure,

in which the individual P3HT chains are stacked together due to the interaction of the overlapping aromatic rings (π-stacking) and the zipper like connection of the alkyl side chains.[17-19] Careful inspection of the diffractograms reveals important alterations occurring upon the doping reaction. The sharp reflection at 2Θ = 5.3° – corresponding to the distance between the interdigitated chains –, gradually shifts to lower values (larger distances). This phenomenon is a side-effect of the oxidation: as the polymer chains get positively charged, Coulomb repulsion dictates larger interchain distances. Most importantly, appearance of two new reflections at 2Θ = 38.1 and 44.4° clearly confirms the formation of *metallic* silver particles on the P3HT nanofibers.

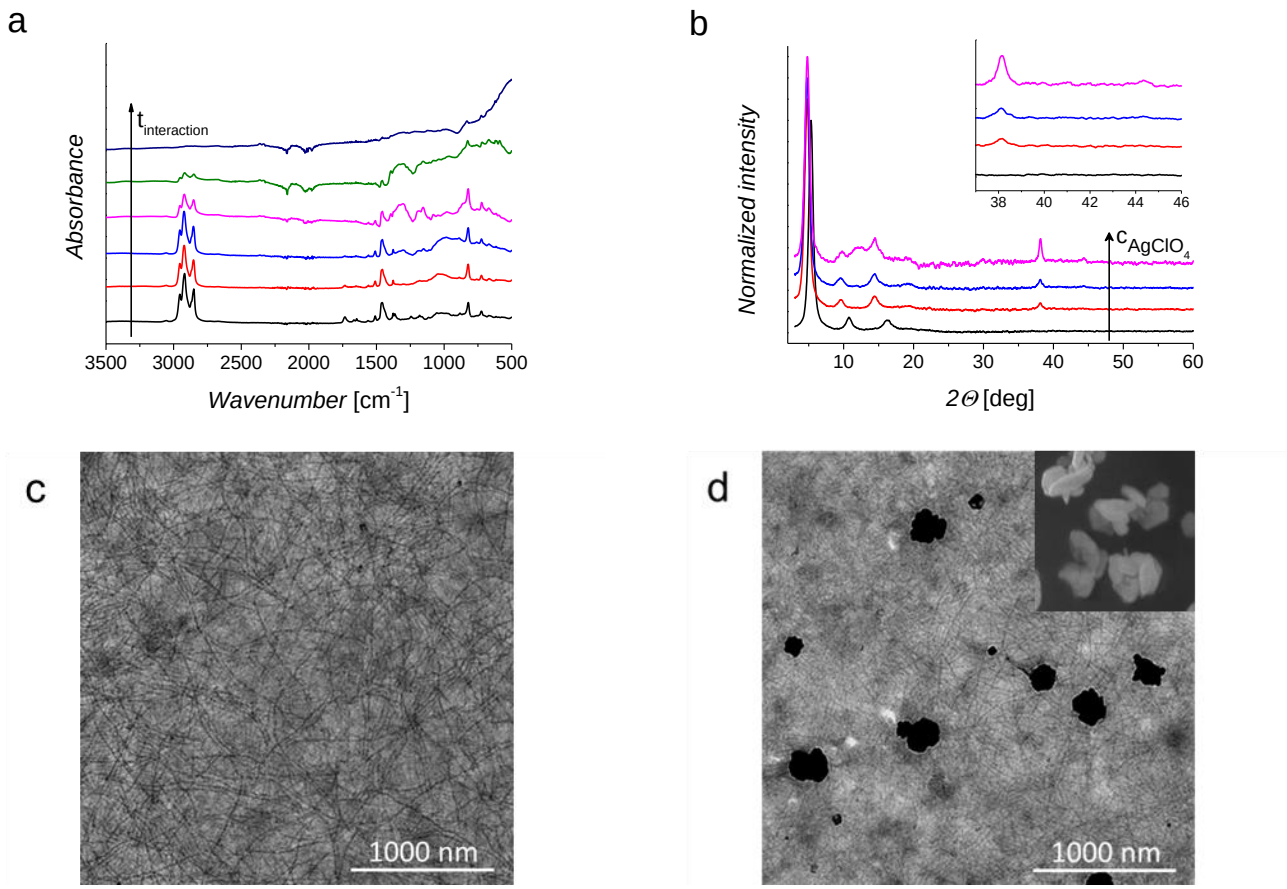

Figure 2. Doping induced structural and morphological changes of the P3HT nanonet. (a) Set of FT-IR spectra, recorded during doping process of P3HT (1 mM $AgClO_4$). (b) XRD spectra of the neutral and $AgClO_4$ doped (1, 5, and 10 mM, respectively) P3HT nanonet. TEM image of (c) neutral and (d) Ag doped P3HT nanonet (the inset shows a SEM image of the silver particles. Note that the same scale bar applies for both images).

As derived from TEM images (Figure 2c-d), recrystallization process results in randomly oriented, 50-60 nm wide and up to micrometer long nanofibers (see also AFM image (Figure S1) in the Supplementary information). Interestingly, at smaller oxidant concentrations Ag appeared as 200-250 nm sized particles on the P3HT network, while 4-500 nm large agglomerates of silver nanoparticles were detected at the highest $AgClO_4$ concentration. What is further important, only a very small fraction of the individual nanofibers is in *direct* contact with the formed silver particles! This observation furnishes at least two important messages. First, the deposited Ag particles do not form a percolation pathway through the bulk nanonet structure (for a further, corroboratory SEM image see Figure S8). Second, since the formation of a fully oxidized P3HT was evidenced by previous spectroscopic methods (i.e., all nanofibers are oxidized), these results indicate an intimate electronic contact among the individual P3HT nanofibers in the self-assembled network.

Thorough thermoelectric characterization of the above samples was carried out to establish structure–property relationships. Although absolute values of both electrical conductivity and Seebeck coefficient were highly dependent on the employed oxidant concentration, some general trends were revealed: (i) neutral P3HT has extraordinary large Seebeck coefficient (~1 mV K^{-1}), but very low electrical conductivity; (ii) electrical conductivity increases by several orders of magnitude upon oxidation, accompanied by the drop of the Seebeck coefficient; (iii) minimum value of the Seebeck coefficient (~60-120 μV K^{-1}) is also dependent on the oxidant concentration; (iv) thermal conductivity varies only slightly upon the change in the oxidation level.

Data in Figure 3 bear all the hallmarks associated with semiconductor thermoelectrics, most importantly that the increase of the doping level (charge carrier concentration) leads to a broad maximum in the power factor.[4,6] Doping level dependent changes of the power factor follows a very similar pattern as alterations in the electrical conductivity, indicating that this latter dictates thermoelectric properties of P3HT.

Benefits of the nanonet structure are highlighted by comparing and contrasting results obtained for the nanonet with those measured for its non-fibrillar counterpart. As seen in Figure 3b, although changes in the value of all the important parameters show similar tendency, both the increase in the electrical conductivity and the decrease in the Seebeck coefficient are *much slower* for the bulk sample. This trend is in good coherence with the previous results: self-assembly of P3HT nanofibers leads to a porous network with good electronic connection among the individual fibers and enough space within the layer for electrolyte penetration.

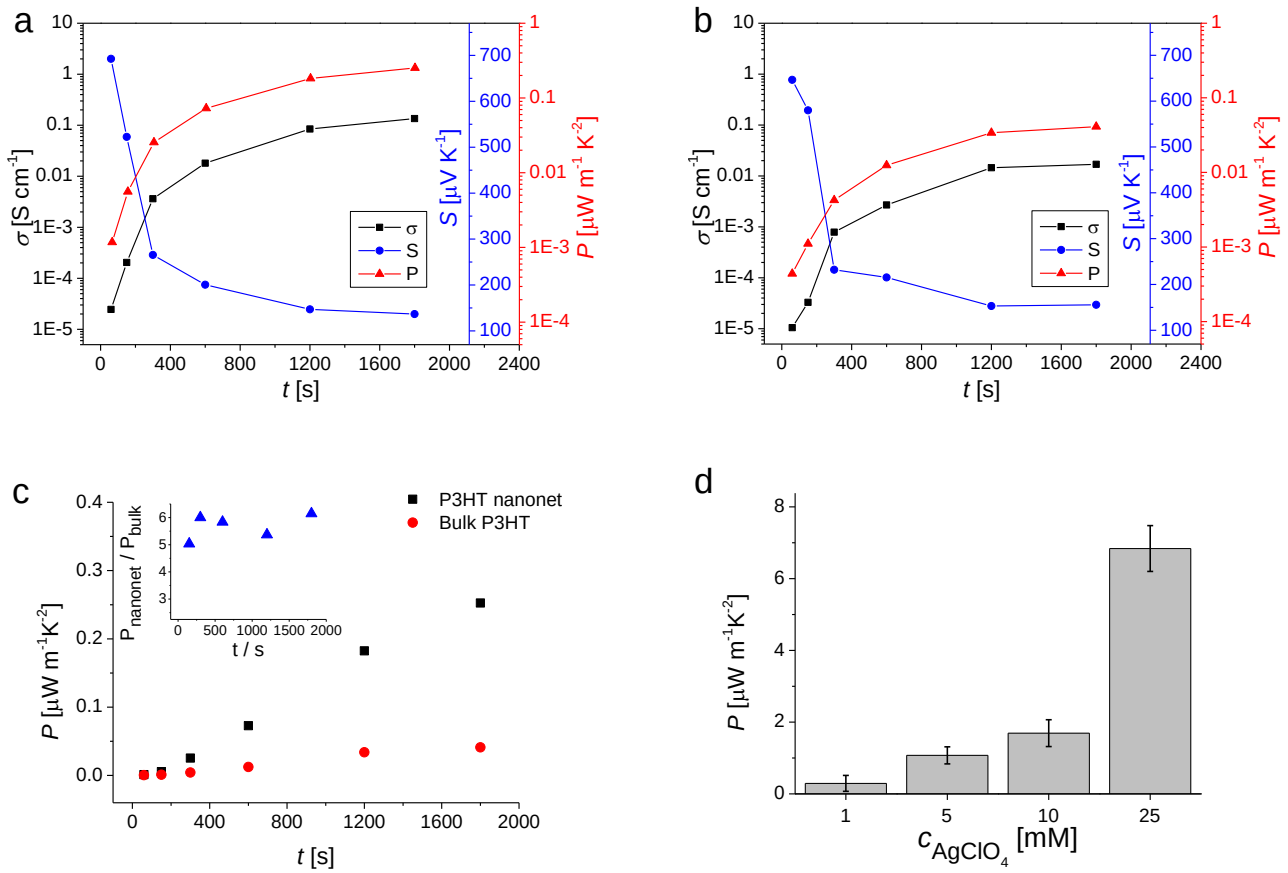

Figure 3. Doping level dependent thermoelectric properties of (a) P3HT nanonet (b) bulk P3HT. (c) Comparison of the power factors measured for the bulk and nanonet structured P3HT, doped with 1 mM $AgClO_4$ solution. (d) Maximum power factor of the P3HT nanonet at different oxidant concentrations.

As for the *value* of the parameters, while the Seebeck coefficient is not affected significantly by the nanoscale morphology, a six fold growth was observed in the power factor upon nanofiber formation (Figure 3c). This increment predominantly originates from the enhanced electrical conductivity, caused by at least three factors: the highly-ordered, crystalline supramolecular structure, the 1D nanofiber morphology, and the intimate electrical contact between the individual nanofibers in the nanonet structure. Importantly, this difference seems to be independent from the oxidant concentration (at least under our conditions, see the inset of Figure 3c), indicating that doping induced structural changes (as deduced from XRD and FT-IR) does not affect deleteriously the beneficial supramolecular structure.

Since the power factor showed monotonous rise (see Figure 3d and Figure S9) with the increasing concentration, experiments were expanded to the concentrated $AgClO_4$ solution (~25 mM). For this heavily doped (doping level of about 0.40, confirmed by EDX measurements (see Figure S10) samples, electrical conductivity of 18.3±1.5 S cm^{-1} and a relatively high Seebeck coefficient, 61.1±2.0 μV K^{-1} was registered. As a result, the best power factor obtained for the P3HT nanonet (~6.84±0.64 μW$m^{-1}K^{-2}$) was about 50 times higher than the highest value, reported earlier for P3HT.[24]

Preliminary studies on the thermal conductivity – performed by the 3ω method – resulted similar values to those published for bulk P3HT[25] (0.45 W$m^{-1}K^{-1}$ for the neutral polymer, reaching a value of 0.80 W$m^{-1}K^{-1}$ for the most heavily doped sample). Importantly, this

value is far below the thermal conductivity of silver metal (~ 400 W $m^{-1}K^{-1}$),[26] indicating that the contribution of the in situ formed silver particles is negligible.

Conclusions

In summary, we conclude that the benefits of the nanonet structure manifest in an enhanced electrical conductivity, evidently rooted in the improved charge carrier mobility. The highest power factor was obtained for the most heavily doped sample. Considering the low thermal conductivity of the fully doped P3HT nanonet, a ZT value of about 0.0026 was obtained at room temperature. Importantly, this is far the highest value reported for P3HT, emphasizing the significance of the supramolecular structure and morphology in CP thermoelectrics. In fact, thermoelectric performance of the fully doped P3HT approaches the best values reported for P3HT based composites[7,10,25,27,28].

We may envision that supramolecular engineering of CPs with high intrinsic charge carrier mobility leads to previously unforeseen ZT values in the future. Such studies in our laboratory are in progress and will be reported soon.

Experimental

P3HT was prepared by oxidative chemical polymerization: chloroform based 3-hexylthiophene and $FeCl_3$ solutions were mixed at final reagent concentrations of 0.1 and 0.25 M, respectively. The continuously stirred reaction mixture was kept in a closed vessel on ice bath for 6 hours. To remove the traces of the oxidant, the precipitated P3HT was washed repeatedly with ethanol. The final product was dried in air, at room temperature.[12]

Whisker method[17-19] was employed to form nanofibers from the bulk polymer. As the first step, a larger molecular weight fraction of P3HT was Soxhlet extracted by tetrahydrofuran (THF). After evaporating the solvent, the polymer was re-dissolved in a 9:1 ratio anisole/chloroform mixture (2.5 g dm^{-3}). The solution was heated to 70 °C and then instantly cooled down to room temperature on ice bath. See further details of both the synthesis and characterization in the Supplementary Information (Figure S1).

P3HT nanonets were formed by drop casting the P3HT solution on plastic substrates (2 cm x 2.5 cm size), previously patterned with 4 gold stripes for 4 point probe electrical measurements. Non-fibrillar thin films were formed similarly from toluene based solution (2.5 g dm^{-3}) of the chemically prepared P3HT for comparison.

Oxidation of the neutral polymer films was performed by immersing them into nitrobenzene based $AgClO_4$ solutions. At a given oxidant concentration, doping level of P3HT was controlled by the reaction time (immersion time). Subsequently, excess of the oxidant was removed by nitrobenzene rinsing.

During the simultaneous in situ spectral and conductance measurements, a special indium tin oxide (ITO)-coated glass working electrode (Figure S2) (IAME, Abtech) was employed in a custom designed electrochemical cell.[20]

FT-IR studies were performed using a Bio-Rad Digilab Division FTS-65A/896 Fourier transform infrared spectrometer equipped with a Harrick's Meridian® SplitPea single reflection diamond attenuated total reflectance (ATR) accessory. All infrared spectra were recorded between 400 and 4000 cm^{-1}, at 4 cm^{-1} optical resolution, averaging 512 interferograms.

Raman spectroscopic studies were performed on a DXR Raman Microscope using a red laser (λ=780 nm), operating at 1 mW laser power.

For transmission electron microscopic (TEM) investigations, P3HT was drop casted on copper mesh TEM grids covered by carbon film. Ag-doping occurred in situ on the P3HT coated grids according to the above described method. A FEI Tecnai G2 20 X-Twin type instrument, operating at an acceleration voltage of 200 kV was used.

Scanning electron microscopic (SEM) images were recorded by a Hitachi S-4700 field emission scanning electron microscope, operating at an acceleration voltage of 10 kV.

XRD spectra were recorded between 2Θ = 3-80° at 1 °C minute-1 scan rate by a Rigaku Miniflex II instrument, operating with a Cu Kα1 radiation source (λ= 0.1541 nm).

AFM images were recorded by a Digital Instruments Atomic Force Microscope Nanoscope III in tapping mode.

Measurement of the Seebeck coefficient was carried out using a custom designed setup (Figure S3). Electrical conductivity of the samples was determined by the 4 point method, using a Keithley 2400 type general purpose source meter. Three samples were prepared at each concentration and all of them were measured three times (9 data points).

Semi-quantitative measurement of the thermal conductivity was performed using the differential 3ω-method. Sinusoidal input current was applied to a ~20 μm wide gold heater. The 3ω-voltage was measured as a function of the sinusoidal frequency.

Acknowledgements

Financial support from the National Development Agency, through the project „TÁMOP-4.2.2.A-11/1/KONV-2012-0047 Biological and Environmental Responses by new functional materials" is gratefully acknowledged. This research was also supported by the European Union and the State of Hungary, co-financed by the European Social Fund in the framework of TÁMOP 4.2.4. A/2-11-1-2012-0001 'National Excellence Program' (B.E.).

Notes and references

1. F. J. DiSalvo, *Science*, 1999, **285,** 703.
2. T. M. Tritt, M. A. Subramanian, *MRS Bull*, 2006, **31,** 188.
3. T. O. Poehler, H. E. Katz, *Energy Environ.Sci.*, 2012, **5,** 8110.
4. O. Bubnova, Z. U. Khan, A. Malti, S. Braun, M. Fahlman, M. Berggren and X. Crispin, *Nat Mater*, 2011, **10,** 429.
5. G. Kim, L. Shao, K. Zhang and K. P. Pipe, *Nat Mater*, 2013, **12,** 719.
6. O. Bubnova, Z. U. Khan, H. Wang, S. Braun, D. R. Evans, M. Fabretto, P. Hojati-Talemi, D. Dagnelund, J. Arlin, Y. H. Geerts, S. Desbief, D. W. Breiby, J. W. Andreasen, R. Lazzaroni, W. M. Chen, I. Zozoulenko, M. Fahlman, P. J. Murphy, M. Berggren and X. Crispin, *Nat Mater*, 2014, **13,** 190.
7. C. Bounioux, P. Diaz-Chao, M. Campoy-Quiles, M. Martin-Gonzalez, A. R. Goni, R. Yerushalmi-Rozen and C. Muller, *Energy Environ.Sci.*, 2013, **6,** 918.
8. J. Sun, M. -. Yeh, B. J. Jung, B. Zhang, J. Feser, A. Majumdar and H. E. Katz, *Macromolecules*, 2010, **43,** 2897.
9. D. Kim, Y. Kim, K. Choi, J. C. Grunlan and C. Yu, *ACS Nano*, 2010, **4,** 513.
10. Y. Du, S. Z. Shen, K. Cai and P. S. Casey, *Progress in Polymer Science*, 2012, **37,** 820.

11. M. Ocypa, M. Ptasinska, A. Michalska, K. Maksymiuk and E. A. H. Hall, *J Electroanal Chem*, 2006, **596,** 157.
12. E. Pintér, Z. A. Fekete, O. Berkesi, P. Makra, Á Patzkó and C. Visy, *J.Phys.Chem.C*, 2007, **111,** 11872.
13. E. Pintér, R. Patakfalvi, T. Fülei, Z. Gingl, I. Dékány and C. Visy, *J Phys Chem B*, 2005, **109,** 17474.
14. P. Brocorens, A. Van Vooren, M. L. Chabinyc, M. F. Toney, M. Shkunov, M. Heeney, I. McCulloch, J. Cornil and R. Lazzaroni, *Adv Mater*, 2009, **21,** 1193.
15. B. Russ, M. J. Robb, F. G. Brunetti, P. L. Miller, E. E. Perry, S. N. Patel, V. Ho, W. B. Chang, J. J. Urban, M. L. Chabinyc, C. J. Hawker and R. A. Segalman, *Adv Mater*, 2014, **26,** 3473.
16. H. Tseng, H. Phan, C. Luo, M. Wang, L. A. Perez, S. N. Patel, L. Ying, E. J. Kramer, T. Nguyen, G. C. Bazan and A. J. Heeger, *Adv Mater*, 2014, **26,** 2993.
17. S. Samitsu, T. Shimomura, S. Heike, T. Hashizume and K. Ito, *Macromolecules*, 2008, **41,** 8000.
18. G. Lu, L. Bu, S. Li and X. Yang, *Adv Mater*, 2014, **26,** 2359.
19. K. M. Coakley, B. S. Srinivasan, J. M. Ziebarth, C. Goh, Y. Liu and M. D. McGehee, *Advanced Functional Materials*, 2005, **15,** 1927.
20. E. Peintler-Kriván, P. S. Tóth and C. Visy, *Electrochem.Commun.*, 2009, **11,** 1947.
21. M. Skompska, A. Szkurlat, A. Kowal and M. Szklarczyk, *Langmuir*, 2003, **19,** 2318.
22. L. F. Cházaro-Ruiz, A. Kellenberger and L. Dunsch, *J Phys Chem B*, 2009, **113,** 2310.
23. M. Baibarac, M. Lapkowski, A. Pron, S. Lefrant and I. Baltog, *J.Raman Spectrosc.*, 1998, **29,** 825.
24. Y. Xuan, X. Liu, S. Desbief, P. Leclère, M. Fahlman, R. Lazzaroni, M. Berggren, J. Cornil, D. Emin and X. Crispin, *Phys.Rev.B*, 2010, **82,** 115454.
25. M. He, J. Ge, Z. Lin, X. Feng, X. Wang, H. Lu, Y. Yang and F. Qiu, *Energy Environ.Sci.*, 2012, **5,** 8351.
26. W. J. Parker, R. J. Jenkins, C. P. Butler and G. L. Abbott, *J.Appl.Phys.*, 1961, **32,** 1679.
27. Y. Du, K. F. Cai, S. Z. Shen and P. S. Casey, *Synth.Met.*, 2012, **162,** 2102.
28. Y. Du, S. Z. Shen, W. D. Yang, K. F. Cai and P. S. Casey, *Synth.Met.*, 2012, **162,** 375.

